

SN 2024iss: Double-Peaked Light Curves and Implications for a Yellow Supergiant Progenitor

Masayuki Yamanaka¹, Takahiro Nagayama², and Tsukiha Horikiri³

¹Amanogawa Galaxy Astronomy Research Center (AGARC), Graduate School of Science and Engineering, Kagoshima University, 1-21-35 Korimoto, Kagoshima, Kagoshima 890-0065, Japan

²Graduate School of Science and Engineering, Kagoshima University, 1-21-35 Korimoto, Kagoshima, Kagoshima 890-0065, Japan

³Department of Physics and Astronomy, Faculty of Science, Kagoshima University, 1-21-35 Korimoto, Kagoshima, Kagoshima 890-0065, Japan

*E-mail: yamanaka@sci.kagoshima-u.ac.jp

Received (reception date); Accepted (acceptation date)

Abstract

We report the multi-band photometric observations of the Type IIb supernova (SN) 2024iss with ultra-violet (UV), optical, and near-infrared (NIR) wavelengths starting one day after the explosion. The UV and optical light curves show the first peak two days after the explosion date. Following a first peak, a secondary maximum is observed in the optical and NIR bands, similar to SNe IIb with double-peaked light curves. The quasi-bolometric light curve shows the fast decay until a week after the explosion. From the analysis of the bolometric light curve, the ejecta mass and kinetic energy are estimated to be $M_{ej} = 2.8 \pm 0.6 M_{\odot}$ and $E_{kin} = 9.4 \pm 4.1 \times 10^{50}$ erg. The mass of the radioactive ^{56}Ni is estimated to be $M(^{56}\text{Ni}) = 0.2 M_{\odot}$. Fitting a blackbody function to the spectral energy distribution reveals that the photospheric temperature exhibits a rapid exponential decline during the first week after the explosion. An analytic model describing the cooling emission after shock breakout provides a reasonable explanation for the observed temperature evolution. From these ejecta parameters, we calculated the progenitor radius to be $R_{pro} = 50 - 340 R_{\odot}$. We conclude that these explosion properties are consistent with a core-collapse explosion from a yellow supergiant (YSG) progenitor.

Key words: supernovae: general — supernovae: individual (SN 2024iss) — supergiants

1 Introduction

Core-collapse supernovae (CC SNe) occur at the final stage of the stellar evolution of the massive star. Observational properties of some CC SNe are explained by the theoretical explosion scenario for the stripped-envelope progenitor (Nomoto et al. 1993; Woosley et al. 1994). The progenitors of Type IIb SNe have a thin hydrogen envelope, although it is quite ambiguous how the progenitor strips off the envelope through the stellar evolution (Smith et al. 2011; Sana et al. 2012). Observational research of Type IIb SNe could

provide an important key to approaching this problem.

The cooling emission has been observed in the light curves of Type IIb SNe 1993J (Richmond et al. 1994), 2011fu (Kumar et al. 2013; Morales-Garoffolo et al. 2015), 2013df (Van Dyk et al. 2014; Morales-Garoffolo et al. 2014; Szalai et al. 2016), 2016gkg (Arcavi et al. 2017; Tartaglia et al. 2017), and 2020bio (Pellegrino et al. 2023) in optical and ultra-violet (UV) wavelengths. The emission comes from the cooling envelope after the shock breakout. After the cooling phase, the secondary maximum is normally observed. The photospheric temperature is higher in earlier

phases, and it rapidly decreases. From the analysis of the cooling emission (Morales-Garoffolo et al. 2014; Tartaglia et al. 2017; Pellegrino et al. 2023) and the pre-explosion images (Aldering et al. 1994; Crockett et al. 2008; Van Dyk et al. 2014), the progenitor is proposed as a yellow supergiant (YSG) star. However, there are no comprehensive photometric analyses including the near-infrared (NIR) data up to date.

SN 2024iss was discovered at 14.6 magnitude by the Gravitational-wave Optical Transient Observer (GOTO; Steeghs et al. 2022) on May 12.9 in 2024 (UT) (O’Neill et al. 2024). This SN was identified as a typical Type IIb SN by two-epoch spectroscopic observations (Srivastav et al. 2024b). The last non-detection magnitude was obtained as 19.5 mag on May 11.9 by the GOTO collaboration (O’Neill et al. 2024). It means that the light curve shows a rapid rise during a day. From this constraint, we define that the breakout time ($t = 0$ d) of this object was at May 12.4 (UT) with an uncertainty of ~ 0.5 day.

The host galaxy of SN 2024iss is faint and compact (Godwin et al. 1983). The uncertainty of the distance is very large. We adopted the distance of 14.1 Mpc, converted by the redshift $z = 0.003334$ reported by (O’Neill et al. 2024). The corresponding distance modulus, $\mu = 30.7$. In the case of the large distance (19.7 Mpc), the peak absolute magnitude of SN 2024iss was -18.2 mag in g -band, which indicates the very luminous for SN IIb. In this Letter, we adopted the former distance for the conservative estimation of the luminosity. We also adopted a Galactic extinction of $A_V = 0.027$ (Schlafly & Finkbeiner 2011) throughout this Letter.

In this Letter we will present the observations and data reduction in §2, the photometric results and comparison of the quasi-bolometric light curves with other objects in §3, and the analysis of the spectral energy distribution and the evolution of the photospheric temperature in §4. Finally, we present the conclusion in §5.

2 Observations & data reduction

We simultaneously obtained the NIR and optical imaging data on eight nights from May 15.5 to Jun 13.6 in the g , i , J , H , and K_s bands with the kSIRIUS+gi camera (Nagayama & Nakaya 2024) attached to the Kagoshima 1-m telescope at the Iriki Observatory.

We carried out the data reduction through the standard manner using *IRAF* (Tody 1986; Tody 1993). After that, we performed the point spread function (PSF) photometry of SN 2024iss and the reference stars using the *DAOPHOT* package (Stetson 1987). We performed the photometric calibration of these data using the Pan-

STARRS (PS1; Chambers et al. 2016) and Two Micron All Sky Survey (2MASS; Cutri et al. 2003) catalogs.

We also used the public g and r -band photometric data from the Zwicky Transient Facility (ZTF; Bellm et al. 2019) survey, and we took the data from the Automatic Learning for the Rapid Classification of Events (ALeRCE; Sánchez-Sáez et al. 2021) site. The first data point was obtained at nine hours after the discovery on May 13.4 (Pérez-Fournon et al. 2024). We confirmed the consistency between the Kagoshima and ZTF g -band light curves, indicating negligible contamination from the host galaxy. We did not apply template subtraction to the photometric data. We also performed the aperture photometry of the public optical and UV imaging data, obtained on 19 epochs from May 13.6 to Jun 23.0 using the UVOT at the Neil Gehrels Swift Observatory (Roming et al. 2005) in $uvw2$, $uvm2$, $uvw1$, U , B , and V -band. We adopted the zeropoints and calibration database from Breeveld et al. (2011). Template subtraction was not performed for the UVOT data. The multi-band light curves are shown in Figure 1.

3 Results

In the UV and optical wavelengths, the $uvw2$, $uvm2$, $uvw1$, U , g , B , V , and r -band light curves exhibit the first peak around $t \sim 2$ d. After that, the secondary maximum is found at $t \sim 17$ d in the g and r bands, and at $t \sim 22$ d in the K_s -band. The longer-wavelength band light curves reach the maximum date later. This fact is consistent with the trend seen in the normal stripped envelope SNe (Bianco et al. 2014; Ergon et al. 2014).

We present the procedure of constructing the quasi-bolometric light curve and analyzing the emission at its first peak. We converted the observed magnitudes into flux densities using the conversion factors provided by Fukugita et al. (1996), Bessell et al. (1998) and Tokunaga & Vacca (2005), and obtained the spectral energy distribution. Using the central wavelength of each passband function (Fukugita et al. 1996; Bessell 1990), we calculated the quasi-bolometric light curves using the distance of 14.1 Mpc. The Galactic extinction was corrected for (Schlafly & Finkbeiner 2011). The extinction in the host galaxy is negligible, as indicated by the non-detection of sodium absorption lines in the spectra (Srivastav et al. 2024a; Srivastav et al. 2024b). We plotted the quasi-bolometric light curve of SN 2024iss in Figure 2. The light curves were compared with those of other Type IIb SNe (Richmond et al. 1994; Marion et al. 2014; Morales-Garoffolo et al. 2014; Morales-Garoffolo et al. 2015; Tartaglia et al. 2017).

Light curve properties were extracted by fitting the light

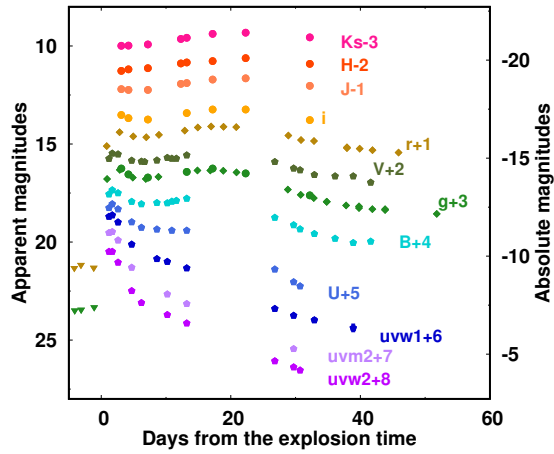


Fig. 1. The UV, optical, and near-infrared light curves of SN 2024iss. The left-side vertical axis denotes the apparent magnitude and the right-side one does the absolute magnitude. The distance modulus was adopted for $\mu = 30.7$ which was converted from the redshift of $z=0.0033$ (O’Neill et al. 2024). The filled-circle symbols denote the photometric point obtained using the kSIRIUS+gi camera. The pentagon-shape symbol denotes data obtained by UVOT. The diamond-shape symbol denotes data obtained by ZTF. The downward triangle denotes the upper-limit magnitude obtained by ZTF. The uvw_2 , uvm_2 , uvw_1 , U , B , V , J , H , and K_s -band magnitudes are in the Vega system, and g , r , and i -band ones in the AB system. Alt text: The horizontal axis is scaled in days from the explosion.

curves with a combined second-order polynomial and exponential function. The fit accurately describes the observed data. The uncertainty is primarily attributed to the distance. The peak luminosity of SN 2024iss is determined to be $5.1 \times 10^{42} \text{ erg s}^{-1}$ at $t = 3.5$ d. Thereafter, the luminosity exhibited a rapid decline to $2.5 \times 10^{42} \text{ erg s}^{-1}$ at $t = 7.6$ d. We defined as the cooling phase until this epoch. The light curve evolution was nearly flat. The first peak luminosity is higher than that of SNe 1993J and 2016gkg during the comparable evolutionary phases. We will present the analysis of the progenitor properties using the light curve in §4.2.

The secondary maximum was marginally detected, with its luminosity of $\sim 2.6 \times 10^{42} \text{ erg s}^{-1}$ at $t = 15.3$ d. The secondary maximum was also much higher than those of other objects, and the rise time is quite shorter than those of the objects. From these properties, we will discuss the ejecta properties of this object in §4.1.

We calculated the temporal evolution of the fraction of the UV and the NIR luminosity fraction against the bolometric light curve. The UV emission fraction shows a rapid decline until $t = 7$ d from $\sim 40\%$ to $\sim 30\%$. Thereafter, it linearly declines to below $\sim 10\%$ at $t = 23$ d. The NIR emission fraction shows a rapid rise to the 20% until $t = 7$ d, and it is larger than that of UV after $t = 10$ d. Finally, the NIR emission reaches $\sim 40\%$ around $t = 30$ d. This means that the NIR component is essentially

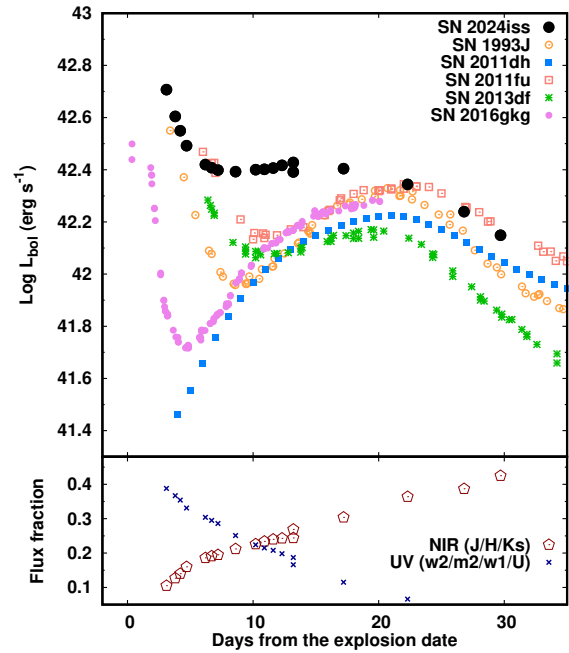


Fig. 2. (Upper panel) The quasi-bolometric light curve of SN 2024iss compared with those of SNe 1993J (Richmond et al. 1994), 2011dh (Marion et al. 2014), 2011fu (Morales-Garofolo et al. 2015), 2013df (Morales-Garofolo et al. 2014) and 2016gkg (Tartaglia et al. 2017). The integration of each band flux was performed using the central wavelength of each band. The Galactic extinction and the distance were corrected for. (Lower panel) The evolution of the UV and NIR fraction. The UV fraction is denoted by cross-shaped symbols in blue, and NIR is denoted by open pentagons in red. Alt text: In the upper panel, the vertical axis shows the quasi-bolometric luminosity in logarithmic scale, in units of erg per second. In the lower panel, the vertical axis shows the fraction of the UV and NIR band flux relative to the total luminosity. The horizontal axis is scaled in days from the explosion.

important for the bolometric correction after the cooling phase before the radioactive peak.

We classify SN 2024iss based on the publicly available spectrum obtained by Srivastav et al. (2024b). The spectra are shown in Figure 3. The blueshifted absorption lines of $H\alpha$ and $He\ I\ \lambda 5876$ are identified in the spectrum. Comparing this spectrum with those of the well-studied Type IIb SNe 1993J (Filippenko et al. 1993) and 2011dh (Marion et al. 2014), we find similar absorption features of hydrogen and helium. This strongly suggests that SN 2024iss is also a Type IIb. The measured expansion velocity of the $H\alpha$ line is $15,000 \text{ km s}^{-1}$, which is consistent with the typical velocities observed in Type IIb SNe (Pastorello et al. 2008; Marion et al. 2014; Medler et al. 2022).

4 Discussion

4.1 Ejecta properties

The ejecta mass and kinetic energy can be estimated based on the light curve timescale and the expansion velocity, us-

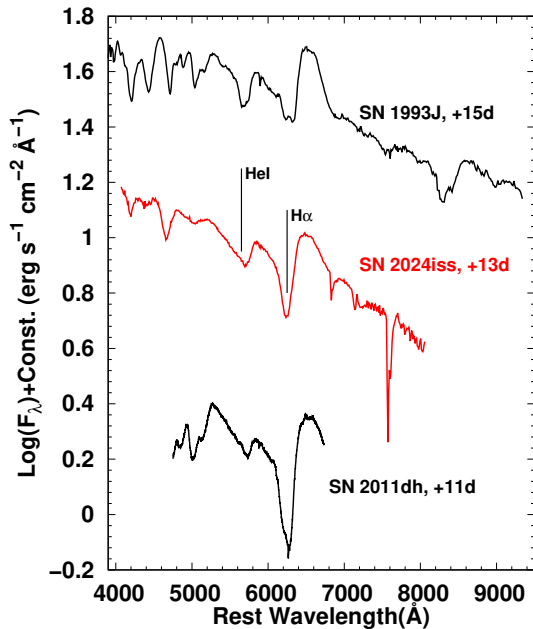


Fig. 3. Optical spectrum of SN 2024iss observed by Srivastav et al. (2024b). It is compared with that of SNe 1993J (Filippenko et al. 1993) and SNe 2011dh (Marion et al. 2014). The wavelength of the host galaxy was corrected to the rest frame using the redshift presented by each literature. The absorption lines of $H\alpha$ and $He I$ are identified, indicating that SN 2024iss is classified as a Type IIb. Alt text: The vertical axis shows the flux in logarithmic scale, in units of erg per second per square centimeter per Angstrom. The horizontal axis shows the wavelength in units of Angstrom.

ing the relation described by Arnett (1982). The rise time, representing the timescale to the peak, was calculated to be $t_{rise} = 15.3$ d, by fitting the function described in §3 to the rising part in the bolometric light curve. We used the $H\alpha$ line velocity of 15000 km s^{-1} from the measurement presented in §3. For the conservative estimate, we adopted a 20% error for these measurements.

The scaling-law method (Arnett 1982) was employed to obtain the kinetic energy (E_{kin}) and the ejecta mass (M_{ej}) of SN 2024iss. We used the kinetic energy $E_{kin} = 8.2 \times 10^{50}$ erg and $M_{ej} = 2.7 M_{\odot}$ of SN 2011dh (Bersten et al. 2012) as reference values to obtain properties of SN 2024iss. The line velocity of SN 2011dh was $v(H\alpha) = 13000 \text{ km s}^{-1}$ around at maximum, and the rise time of SN 2011dh was $t_{rise} = 22$ d (Marion et al. 2014). From these parameters, we derived the kinetic energy of $E_{kin} = 9.4 \pm 4.1 \times 10^{50}$ erg and ejecta mass of $M_{ej} = 2.8 \pm 0.6 M_{\odot}$. The uncertainty in the rise time and line velocity of SN 2024iss contributes to the error. We will use these parameters for an analysis of the progenitor in §4.2.

The mass of the radioactive ^{56}Ni is dependent on a peak luminosity and a rise time of the bolometric light curve (Arnett 1982). In the case of Type IIb SNe with a double-peaked light curve, the secondary maximum can be

explained by the presence of ^{56}Ni . Based on the secondary peak luminosity of $\sim 2.6 \times 10^{42} \text{ erg s}^{-1}$ and the rise time of $t = 15.3$ d, the radioactive nickel mass of SN2024iss is estimated to be $M(^{56}\text{Ni}) = 0.2 M_{\odot}$. This value is consistent with the range of ^{56}Ni masses observed in Type IIb SNe (Lyman et al. 2016).

4.2 Analysis of the cooling phase

We constructed the spectral energy distribution (SED) of SN2024iss for the seven epochs in the UV, optical, and NIR wavelengths (see Figure 4). The central wavelengths of the $uvw2$, $uvm2$, $uvw1$, U , B , V , g , i , J , H , and K_s -band data were used in order to convert the magnitudes to the flux density. We performed the black-body fitting to the SED using the least squares method. The estimated photospheric temperature and radius are shown in Figure 5. While the temperature rapidly decreases with time, the photospheric radius gradually increases.

We also attempted to fit the theoretical model to the evolution of the temperature. We used the blue supergiant (BSG) progenitor model from Nakar & Sari (2010) and the yellow supergiant (YSG) progenitor model from Milisavljevic et al. (2013), the latter of which was originally proposed by Nakar & Sari (2010). In these models, the temperature evolution depends on the ejecta mass, the ejecta kinetic energy, and the progenitor radius. The temperature evolution was well explained by both models within the uncertainty. From the BSG model, we estimated the progenitor radius to be, $R = 340 \pm 40 R_{\odot}$ while from the YSG model, we estimated it to be $R = 50 \pm 5 R_{\odot}$. Based on these fits, we conclude that the progenitor radius is likely $50 - 340 R_{\odot}$.

For other SNe IIb, the progenitor radii were estimated to be $\sim 450 R_{\odot}$ for SN 2011fu (Morales-Garoffolo et al. 2015), $64 - 169 R_{\odot}$ for SN 2013df (Morales-Garoffolo et al. 2014), and $48 - 124 R_{\odot}$ for SN 2016gkg (Tartaglia et al. 2017) using the similar method. Our estimated progenitor size is consistent with that of SNe 2013df and 2016gkg, but smaller than that of SN 2011fu. Considering the systematic difference of the model, the progenitor size of SN 2024iss was consistent with the range of Type IIb SNe.

5 Conclusion

We present the multi-band light curves of SN 2024iss obtained in UV, optical, and NIR wavelengths simultaneously. From the quasi-bolometric light curve, we estimated the light-curve properties as follows. The radioactive ^{56}Ni mass was $0.2 M_{\odot}$, the total ejecta mass was $M_{ej} = 2.8 \pm 0.6 M_{\odot}$, and the kinetic energy of ejecta was

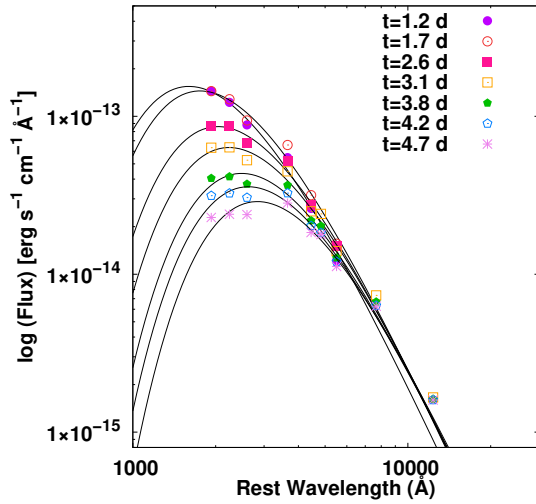


Fig. 4. The spectral energy distribution of SN 2024iss during a week after the explosion between $t = 1.2$ and 4.7 d. the black curves denote the black-body function. Alt text: The vertical axis shows the flux in logarithmic scale, in units of erg per second per square centimeter per Angstrom. The horizontal axis shows the wavelength in units of Angstrom. The evolution of the spectral energy distribution is shown, with each phase is represented by different colors.

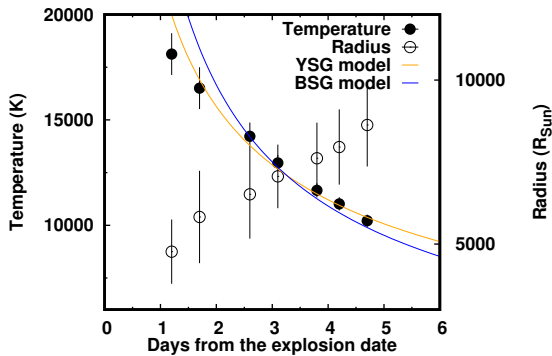


Fig. 5. Evolution of photospheric temperature and radius of SN 2024iss. Black-color filled circle denotes the evolution of the photospheric temperature. The orange curve shows the best-fit solution for the YSG model proposed by Milisavljevic et al. (2013), while the blue curve shows that for the BSG model (Nakar & Sari 2010). The black-color open circle denote the temporal evolution of the photospheric radius. Alt text: The left-side vertical axis shows the temperature in units of kelvin. The right-side axis shows the radius in units of solar radius.

$E_{kin} = 9.4 \pm 4.1 \times 10^{50}$ erg. These ejecta parameters are consistent with those of comparative Type IIb SNe. From the comparison of the temperature evolution with the analytic model, we estimated the progenitor size of SN 2024iss to be $R_{pro} = 50 - 340 R_{\odot}$. It is consistent with the range of Type IIb SNe. From these facts, we concluded that SN 2024iss could be a core-collapse explosion from the yellow (YSG) supergiant (Morales-Garoffolo et al. 2014; Morales-Garoffolo et al. 2015; Tartaglia et al. 2017).

Acknowledgments

We are grateful to graduate and undergraduate students for performing the optical and near-infrared observations. This work was supported by Grant-in-Aid for Scientific Research (C) 22K03676. The Kagoshima University 1 m telescope is a member of the Optical and Infrared Synergetic Telescopes for Education and Research (OISTER) program funded by the MEXT of Japan.

References

- Aldering, G., Humphreys, R. M., & Richmond, M. 1994, *AJ*, 107, 662
- Arcavi, I., Hosseinzadeh, G., Brown, P. J., et al. 2017, *ApJL*, 837, L2
- Arnett, W. D. 1982, *ApJ*, 253, 785
- Bellm, E. C., Kulkarni, S. R., Graham, M. J., et al. 2019, *PASP*, 131, 018002
- Bersten, M. C., Benvenuto, O. G., Nomoto, K., et al. 2012, *ApJ*, 757, 31
- Bessell, M. S. 1990, *PASP*, 102, 1181
- Bessell, M. S., Castelli, F., & Plez, B. 1998, *A&A*, 333, 231
- Bianco, F. B., Modjaz, M., Hicken, M., et al. 2014, *ApJS*, 213, 19
- Breeveld, A. A., Landsman, W., Holland, S. T., et al. 2011, in *American Institute of Physics Conference Series*, Vol. 1358, *Gamma Ray Bursts 2010*, ed. J. E. McEnery, J. L. Racusin, & N. Gehrels (AIP), 373–376
- Chambers, K. C., Magnier, E. A., Metcalfe, N., et al. 2016, *arXiv e-prints*, arXiv:1612.05560
- Crockett, R. M., Eldridge, J. J., Smartt, S. J., et al. 2008, *MNRAS*, 391, L5
- Cutri, R. M., Skrutskie, M. F., van Dyk, S., et al. 2003, *VizieR Online Data Catalog*, II/246
- Ergon, M., Sollerman, J., Fraser, M., et al. 2014, *A&A*, 562, A17
- Filippenko, A. V., Matheson, T., & Ho, L. C. 1993, *ApJL*, 415, L103
- Fukugita, M., Ichikawa, T., Gunn, J. E., et al. 1996, *AJ*, 111, 1748
- Godwin, J. G., Metcalfe, N., & Peach, J. V. 1983, *MNRAS*, 202, 113
- Kumar, B., Pandey, S. B., Sahu, D. K., et al. 2013, *MNRAS*, 431, 308

- Lyman, J. D., Bersier, D., James, P. A., et al. 2016, *MNRAS*, 457, 328
- Marion, G. H., Vinko, J., Kirshner, R. P., et al. 2014, *ApJ*, 781, 69
- Medler, K., Mazzali, P. A., Teffs, J., et al. 2022, *MNRAS*, 513, 5540
- Milisavljevic, D., Margutti, R., Soderberg, A. M., et al. 2013, *ApJ*, 767, 71
- Morales-Garoffolo, A., Elias-Rosa, N., Benetti, S., et al. 2014, *MNRAS*, 445, 1647
- Morales-Garoffolo, A., Elias-Rosa, N., Bersten, M., et al. 2015, *MNRAS*, 454, 95
- Nagayama, T., & Nakaya, H. 2024, in *Society of Photo-Optical Instrumentation Engineers (SPIE) Conference Series*, Vol. 13096, *Ground-based and Airborne Instrumentation for Astronomy X*, ed. J. J. Bryant, K. Motohara, & J. R. D. Vernet, 130963I
- Nakar, E., & Sari, R. 2010, *ApJ*, 725, 904
- Nomoto, K., Suzuki, T., Shigeyama, T., et al. 1993, *Nature*, 364, 507
- O'Neill, D., Godson, B., Killestein, T., et al. 2024, *Transient Name Server AstroNote*, 128, 1
- Pastorello, A., Kasliwal, M. M., Crockett, R. M., et al. 2008, *MNRAS*, 389, 955
- Pellegrino, C., Hiramatsu, D., Arcavi, I., et al. 2023, *ApJ*, 954, 35
- Pérez-Fournon, I., Poidevin, F., Aguado, D. S., et al. 2024, *Transient Name Server AstroNote*, 130, 1
- Richmond, M. W., Treffers, R. R., Filippenko, A. V., et al. 1994, *AJ*, 107, 1022
- Roming, P. W. A., Kennedy, T. E., Mason, K. O., et al. 2005, *Space Sci. Rev.*, 120, 95
- Sana, H., de Mink, S. E., de Koter, A., et al. 2012, *Science*, 337, 444
- Sánchez-Sáez, P., Reyes, I., Valenzuela, C., et al. 2021, *AJ*, 161, 141
- Schlafly, E. F., & Finkbeiner, D. P. 2011, *ApJ*, 737, 103
- Smith, N., Li, W., Filippenko, A. V., & Chornock, R. 2011, *MNRAS*, 412, 1522
- Srivastav, S., Fulton, M., Nicholl, M., et al. 2024a, *Transient Name Server Classification Report*, 2024-1517, 1
- . 2024b, *Transient Name Server Classification Report*, 2024-2046, 1
- Steehls, D., Galloway, D. K., Ackley, K., et al. 2022, *MNRAS*, 511, 2405
- Stetson, P. B. 1987, *PASP*, 99, 191
- Szalai, T., Vinkó, J., Nagy, A. P., et al. 2016, *MNRAS*, 460, 1500
- Tartaglia, L., Fraser, M., Sand, D. J., et al. 2017, *ApJL*, 836, L12
- Tody, D. 1986, in *Society of Photo-Optical Instrumentation Engineers (SPIE) Conference Series*, Vol. 627, *Instrumentation in astronomy VI*, ed. D. L. Crawford, 733
- Tody, D. 1993, in *Astronomical Society of the Pacific Conference Series*, Vol. 52, *Astronomical Data Analysis Software and Systems II*, ed. R. J. Hanisch, R. J. V. Brissenden, & J. Barnes, 173
- Tokunaga, A. T., & Vacca, W. D. 2005, *PASP*, 117, 421
- Van Dyk, S. D., Zheng, W., Fox, O. D., et al. 2014, *AJ*, 147, 37
- Woolley, S. E., Eastman, R. G., Weaver, T. A., & Pinto, P. A. 1994, *ApJ*, 429, 300